Available online at www.sciencedirect.com
SCIENCE DIRECT®
Composites Science and Technology 63 (2003) 1931–1948
COMPOSITES SCIENCE AND TECHNOLOGY
www.elsevier.com/locate/compscitech

Simulation of the three-dimensional non-isothermal mold filling process in resin transfer molding

A. Shojaei[a,*], S.R. Ghaffarian[b,*], S.M.H. Karimian[c]

[a]Chemical & Petroleum Engineering Department, Sharif University of Technology, PO Box 11365/8639, Tehran, Iran
[b]Polymer Engineering Department, Amirkabir University of Technology, Tehran 15875-4413, Iran
[c]Aerospace Engineering Department, Amirkabir University of Technology, Tehran 15875-4413, Iran

Received 28 August 2002; received in revised form 25 February 2003; accepted 20 March 2003

Abstract

Numerical simulation of resin transfer molding (RTM) is known as a useful method to analyze the process before the mold is actually built. In thick parts, the resin flow is no longer two-dimensional and must be simulated in a fully three-dimensional space. This article presents numerical simulations of three-dimensional non-isothermal mold filling of the RTM process. The control volume/finite element method (CV/FEM) is used in this study. Numerical formulation for resin flow is based on the concept of nodal partial saturation at the flow front. This approach permits to include a transient term in the working equation, removing the need for calculation of time step to track the flow front in conventional scheme. In order to compare the results of the nodal partial saturation concept with the conventional method, a numerical scheme based on the quasi-steady state formulation is also presented. The computer codes developed based on both numerical formulations, allow the prediction of flow front positions; and pressure, temperature and conversion distributions in three-dimensional molds with complicated geometries. The validity of the two schemes is evaluated by comparison with analytical solutions of simple geometries. In all instances excellent agreement is observed. Numerical case studies are provided to demonstrate the effectiveness of the developed computer codes. The results show that the numerical procedure based on the nodal partial saturation concept, developed in this study, provides numerically valid and reasonably accurate predictions.

Keywords: A. Polymer-matrix composites; E. Resin transfer molding (RTM); Control volume/Finite element

1. Introduction

The resin transfer molding (RTM) process has become an efficient and attractive technique to produce high quality fiber-reinforced composite parts. Low molding pressure (typically below 5 atm) is a major advantage of the RTM process. This ability allows it for the use of low cost mold and makes the process to be cost effective method to fabricate composite parts. RTM has also the capability of manufacturing the composites with large size and complex shape in a short cycle time. A typical RTM process consists of two important stages which occur sequentially in a process cycle. First, a reactive resin is injected into the mold to fill the cavity and impregnates the fibrous reinforcement preplaced inside the mold cavity. Due to heat conduction from the mold walls to the fluid resin, energy convection by the fluid, and heat released by chemical reaction, the flow will be non-isothermal during this stage. Second, the curing process which is initiated when the fibrous medium is completely wetted out by the resin.

The mold filling process is a very important step in the resin transfer molding, governing the performance of the final product and tool design. It is affected by several parameters comprising of mold geometry, inlet gate(s) location, injection pressure or flow rate, resin rheology, permeability of fibrous media and temperatures of mold wall and inlet resin. Higher injection pressure decreases the mold filling time, however it may cause mold deformation and fiber washout. Heat transfer from the mold wall decreases the resin viscosity and reduces the mold filling time, but the temperature rise activates the curing reaction, leading to a viscosity increase as the resin polymerizes. An excessive increase

* Corresponding authors. Tel.: +98-21-6165462; fax: +98-21-6022853.
E-mail addresses: akbar.shojaei@sharif.edu (A. Shojaei); rezaghaf@cic.aut.ac.ir (S.R. Ghaffarian).

0266-3538/03/$ - see front matter © 2003 Published by Elsevier Ltd.
doi:10.1016/S0266-3538(03)00161-1

Nomenclature

a	constant in viscosity equation, Eq. (7)
$\boldsymbol{A}$, $\boldsymbol{A}'$	stiffness matrices in flow models
$\boldsymbol{A^T}$,$\boldsymbol{A^\alpha}$	stiffness matrices in heat and species balances, Eqs. (31)–(32)
A_1,A_2	constants in kinetic equation, Eq. (11)
b	constant in viscosity equation, Eq. (7)
$\boldsymbol{B^T}$,$\boldsymbol{B^\alpha}$	force vectors in heat and species balances, Eqs. (31)–(32)
C_p	specific heat
E_1,E_2	activation energies in kinetic equation, Eq. (11)
E_μ	activation energy in viscosity equation, Eq. (7)
f	nodal fill fraction
$\boldsymbol{f}$	fill fraction filled
G	reaction rate
ΔH	heat of reaction
$[J^{-1}]$	inverse of Jacobian matrix
l	length
k	thermal conductivity
$[K]$	permeability tensor
K_{ij}	components of permeability tensor
m_1,m_2	constants in kinetic equation, Eq. (11)
n	outward unit normal surface vector
N	number of sub-time steps
P	pressure
q	flow rate
R	gas constant
$[S]$	matrix of derivatives of the shape functions
t	time
Δt	time step
T	absolute temperature
$\vec{v}$	velocity vector
u, v, w	components of velocity vector
x,y, z	global Cartesian coordinates

Greek letters

α	conversion
β	thermal diffusivity of the resin
δ	mass flux term in Eq. (15)
δ_T	thermal flux term in Eq. (27)
δ_c	species flux term in Eq. (30)
μ	viscosity of resin
μ_0	constant in viscosity equation, Eq. (7)
ϕ	porosity
λ	constant in Eq. (39)
φ	intersection point of an element surface
ρ	density
ω	weight fraction
ϖ	saturation level
ψ	Courant number

Subscripts and superscripts

c	current value
e	element
f	fiber
g	gel
i	node or CV number
max	maximum value
o	old value
r	resin
S	control surface
V	control volume

Notations

ip	integration point
$Int(\ )$	integer value
CV	control volume
SCV	subcontrol volume
SS	surface of subcontrol volume

in temperature leads to gelation of the resin during mold filling and stops the filling process. Optimization of all earlier-mentioned parameters by experimental works is a costly and time-consuming task. Alternatively, computer simulation has become a cost effective tool.

The flow, heat transfer and resin cure are strongly interrelated in the non-isothermal filling process. For example, flow pattern is affected by both heat transfer and cure reaction through the resin viscosity, because the viscosity changes as a function of temperature and conversion. Moreover, flow pattern influences the temperature and degree of cure by the convection of fluid. In order to successfully predict the filling process, the process modeling should correctly incorporate the coupling between these phenomena.

Over the past decade, several researchers have developed computer codes to simulate the filling process under non-isothermal conditions [1–9] (see also the review of this subject presented by Shojaei et al. [10]). In most cases, the simulation has been restricted to a 2.5-D problem in which the flow is assumed 2-D flow while the heat transfer is still 3-D. In such cases, the temperature dependent variable in flow model, viscosity, and the permeability must be averaged in the thickness direction of the cavity. Although the assumption of 2-D flow simplifies the simulation and reduces the computation time, 3-D simulation leads to more accurate and realistic results. It should be noted that 2-D assumption is not valid for thick parts or parts having very low permeability in thickness direction. In such cases, flow as well

as temperature and degree of cure vary significantly through the thickness of mold. Young [11] developed a non-isothermal computer code to simulate the fully 3-D mold filling process of RTM. Lim and Lee [12] also presented a numerical code for simulation of the 3-D non-isothermal filling process and, applied their code to predict the resin flow, temperature distribution, and degree of cure for some 3-D complicated geometries.

The numerical treatment of moving boundary problem is an important issue in the simulation of mold filling. In a broad sense, numerical schemes are developed for either: (1) moving grids, or (2) fixed grids. A moving grid scheme often provides accurate representation of flow front position. However, since the calculation domain should be remeshed at each time step, it is computationally very time consuming, and theoretically very difficult to be coded for the complex shaped mold with inserts or multiple injection gates. Coulter and Guceri [13], and Gauvin and Trochu [14] used numerical simulations based on boundary fitted finite differences. Hourng and Chang [3] also applied a body fitted coordinate transformation in their non-isothermal analysis of filling process to reduce the error encountered due to irregular boundary shapes. Um and Lee [15], and Yoo and Lee [16] developed the boundary element method for mold filling process. A numerical simulation based on finite element method was proposed by Chan and Hwang [1] using quadrilateral elements to study non-isothermal filling but the applications were limited to rectangular molds. These numerical methods were all based on a moving grid scheme. On a fixed grid, Gao et al. [6] employed a computer program using non-conforming finite elements to simulate the non-isothermal filling process. Among the existing numerical techniques, a method based on combination of finite element (FE) and control volume (CV) has become the most versatile and computationally efficient way to solve the filling process. This has been also an attractive method used by several researchers to simulate mold filling of cavities with complex geometry [2,4,5,7,11,12]. In this method one does not need to regenerate the mesh, since a fixed grid scheme is followed. Bruschke and Advani [4] simulated mold filling process using FE/CV formulations. They employed Galerkin finite elements to solve the pressure within the solution domain, and used a control volume approach to find the flow front location at each time step. Lin et al. [2] employed control volume finite element method (CV/FEM). In these methods, a procedure based on quasi-steady concept is used to track the flow front. Therefore, the time step size must be so chosen that the steady state assumption is satisfied at each step. However, Joshi et al. [17] found that the law of mass conservation is violated for 2 and 3-D mold filling situations when using these conventional methods of finite element and control volume, for example, when the Galerkin formulation is used to obtain the pressure field. Such mass imbalance may lead to noticeable error in simulated fill time.

Recently, some researchers have attempted to include the transient term in the flow model enabling one to remove the restriction in selection of time step size [18,19]. Voller and Peng [18] proposed an iterative algorithm on the basis of control volume finite element formulation to search for the flow front location under isothermal condition [18]. Lin et al. [19] developed a finite element formulation based on the concept of partial saturation at flow front and implicit time integration to simulate the isothermal filling process.

The present paper deals with numerical simulations of the 3-D non-isothermal mold filling process, including cure and temperature effects in the context of RTM. The numerical scheme used in this study is an extension of our previous work devoted to the simulation of isothermal case [20,21] in which the mold filling process was simulated based on the nodal partial saturation formulation at the flow front. With respect to conventional quasi-steady state approach, our 3-D simulation resulted in the following two important findings: (1) saving in computational time, and (2) achieving a better accuracy in predicted mold filling time. For the purpose of comparison, a computer code is also developed based on the quasi-steady state formulation to simulate non-isothermal mold filling. The CV/FEM method is used in both cases. Both codes are validated by comparison of their results with analytical solution. The effectiveness of the codes is illustrated by numerical simulation of the non-isothermal mold filling stage of different mold geometries.

2. Theory

2.1. Darcy's law and the continuity equation

The liquid flow through fibrous reinforcement can be regarded as a flow through porous medium. In RTM, the flow through such a medium can be expressed by Darcy's law which is reasonable prediction for low Reynolds number flow regime. It has become the most commonly used equation for modeling flow within the RTM mold, and is used as the momentum equation. This equation is expressed as:

$$\begin{bmatrix} u \\ v \\ w \end{bmatrix} = -\frac{1}{\mu}\begin{bmatrix} K_{xx} & K_{xy} & K_{xz} \\ K_{yx} & K_{yy} & K_{yz} \\ K_{zx} & K_{zy} & K_{zz} \end{bmatrix}\begin{bmatrix} \frac{\partial P}{\partial x} \\ \frac{\partial P}{\partial y} \\ \frac{\partial P}{\partial z} \end{bmatrix} \tag{1}$$

Eq. (1) can be rewritten in tensor notation as:

$$\vec{v} = -\frac{1}{\mu}[K].\nabla P \tag{2}$$

On the basis of partial saturation concept, the mass balance equation for an incompressible fluid flow is expressed as [18–20]:

$$\phi\frac{\partial\varpi}{\partial t} = -\nabla.\vec{v} \tag{3}$$

in which the saturation level, ϖ, is 1 at a fully saturated point, and its value ranges between 0 and 1 at a partially saturated point. If the transient term on the left hand side of the earlier equation is removed, the following equation is obtained for quasi-steady state situation:

$$\nabla\cdot\vec{v} = 0 \tag{4}$$

Eq. (2) may be substituted into Eqs. (3) and (4) to produce single equations of:

$$\phi\frac{\partial\varpi}{\partial t} = \nabla.\left(\frac{1}{\mu}[K]\nabla P\right) \tag{5}$$

and

$$\nabla.\left(\frac{1}{\mu}[K]\nabla P\right) = 0. \tag{6}$$

The solution of these equations requires a set of boundary conditions. The possible boundary conditions could be:

- $P = P_0$ for constant pressure injection or $u = u_0$ for constant velocity injection at the inlet gate;
- $P = 0$ at the flow front; and
- $\frac{\partial P}{\partial\vec{n}} = 0$ at the mold wall.

The resin viscosity is a function of temperature and resin conversion. It decreases when temperature increases however it rapidly increases when conversion increases. The viscosity equation used in this study is the widely used model given as [22]:

$$\mu = \mu_0 e^{E_\mu/RT}\left[\frac{\alpha_g}{\alpha_g-\alpha}\right]^{a+b\alpha} \tag{7}$$

2.2. Energy equation

As the resin flows through the fibrous media, heat transfer takes place between the mold wall, the fiber and the resin in the non-isothermal processes. Therefore, heat transfer model should be applied for fiber and resin phases separately. It has been shown that the thermal equilibrium assumption is valid for slow processes such as RTM in which the resin and fiber have the same temperature at each point [23]. The heat dispersion due to the local fluctuations in the velocity field is also insignificant for low Peclet and Graetz numbers [24]. In these conditions, the energy equation governing heat transfer in fibrous media being impregnated with resin is written as [2]:

$$\rho C_p\frac{\partial T}{\partial t} + \rho_r C_{p_r}\left(\vec{v}\cdot\nabla T\right) = \nabla\cdot k\nabla T + \phi\,\Delta H\dot{G} \tag{8}$$

where the effective thermal conductivity, k, ρ and C_p may be expressed as:

$$k = \frac{k_r k_f}{k_r\,\omega_f + k_f\omega_r} \qquad \rho = \frac{\rho_r\rho_f}{\rho_r\omega_f + \rho_f\omega_r}$$
$$C_p = C_{p_r}\omega_r + C_{p_f}\omega_f \tag{9}$$

in which

$$\omega_r = \frac{\dfrac{\phi}{\rho_f}}{\dfrac{\phi}{\rho_f}+\dfrac{1-\phi}{\rho_r}} \quad \& \quad \omega_f = 1-\omega_r \tag{10}$$

The kinetic model proposed by Kamal and Sourour [25] is used in this study as follows:

$$\dot{G} = \left(A_1 e^{-E_1/RT} + A_2 e^{-E_2/RT}\alpha^{m_1}\right)(1-\alpha)^{m_2} \tag{11}$$

The boundary conditions for energy equation can be stated as:

- $T = T_0$ at the inlet gate;
- $T = T_f$ or $\frac{D}{Dt}\left(f\rho C_p T\right) = f\phi\Delta H\dot{G} + \frac{df}{dt}(1-\phi)\rho_f C_{p_f}\left(T_{f_0}-T\right)$ at the flow front; and
- $T = T_m$ at the mold wall.

As written, the boundary condition imposed at flow front may be expressed either by a constant temperature equal to the temperature of the fiber mat [6,26] or a heat balance equation [2,11]. The left hand side of heat balance equation presents the change of internal energy in a control volume, the first term at the right hand side is the heat of reaction and the second term denotes the heat exchange between the fiber and resin. Antonucci et al. [27] presented another thermal boundary condition named jump equation, including the conductive heat flux across the flow front and being a balance on a surface. Comparison between different boundary conditions provided by Antonucci et al. [27] shows that both the constant temperature and heat balance equation lead to the similar temperature results at the flow front especially at the end of mold filling. We use both constant temperature and heat balance equation given earlier as thermal boundary conditions in the numerical simulation.

2.3. Chemical species equation

Mass conservation of chemical species can be expressed as:

$$\phi\frac{\partial\alpha}{\partial t} + \vec{v}\,.\nabla\alpha = \phi\dot{G} \tag{12}$$

where it is assumed that molecular diffusion of macromolecules is negligible and conversion is dominated by convection of fluid and chemical reaction. The boundary conditions may be given as [2]:

- $\alpha = \alpha_0$ at the inlet gate; and
- $\frac{D}{Dt}(f\alpha) = fG$ at the flow front.

3. Numerical formulation

In the present paper, CV/FEM is used for the numerical solution of the filling problem. This is the most popular method to solve the filling stage due to its simplicity in handling the moving boundary problems. In CV/FEM, a fixed grid approach is used in which there is no need to regenerate the mesh during flow progression. This makes the simulation rapid and effective for complicated geometries compared to moving grid approach. Solution domain is first divided into a finite number of elements enabling a well discretization of the complex geometries, and then, the governing equation is discretized using the control volume method. The combination of geometric flexibility of finite element method with conservation property of the control volume technique makes the CV/FEM a convenient and powerful numerical method for solving the moving boundary problem.

To begin the numerical formulation, the three-dimensional mold cavity is divided into linear, hexahedral elements defined by eight nodes [20]. A single hexahedral element with its local coordinate system is shown in Fig. 1(a). Control volumes are constructed by joining the centers of each face of the elements to the midpoint of edges and to the center of the elements creating polygonal control volumes. Therefore, each element will contain eight control volume octants from eight different control volumes. Each octant is called subcontrol volume (*SCV*) and its surfaces are called subsurfaces (*SS*). The control volume of an interior node would be complete and is comprised of eight *SCV*s, however, the control volume of a boundary node is comprised of less than eight *SCV*s, and would not be complete. A typical element divided into its *SCV*s with one *SCV* removed for the sake of clarity is shown in Fig. 1(b). The six faces of each *SCV* are divided into two groups, those that are coincident with the element faces and those that are in the interior of the element. The latter group will form the surfaces of the control volume and are labeled *A*, *B* and *C* as shown in Fig. 1(b).

The status of each control volume is represented by nodal fill fraction, *f*. The fill fraction for each control volume represents the ratio of occupied volume by the resin to its total pore volume. For an empty control volume $f=0$, and f is 1 when the control volume is completely filled with resin. Solution domain includes all filled control volumes, where pressure is calculated within. In all partially filled or empty control volumes the pressure is zero. According to this approach, the flow front lies over the control volumes where they are adjacent to filled control volumes and are not completely filled. The flow front boundary condition is imposed at these control volumes.

3.1. Flow model

The governing equation, Eq. (5), is integrated over an arbitrary control volume. Divergence theorem then is used to obtain:

$$\phi \frac{\partial}{\partial t}\int\int\int_V \varpi dV = \int\int_S \left(\frac{1}{\mu}[K].\nabla P\right).\boldsymbol{dS} \tag{13}$$

in which differential surface vector, $\boldsymbol{dS}$, has three components dS_x , dS_y and dS_z. On the basis of fill fraction concept, the integral of the left hand side of Eq. (13) for a control volume with volume of V can be replaced with product Vf , hence, the resulting equation would become:

$$\phi V \frac{\partial f}{\partial t} = \int\int_S \left(\frac{1}{\mu}[K].\nabla P\right).\boldsymbol{dS} \tag{14}$$

The integral of Eq. (14) is exact for a control volume and it can be applied over any of them. Element by element assembly procedure makes the best use of the fact that all geometric information is defined on an elemental basis. In this paper, the integrals are evaluated over the elemental *SCV*s which eventually will form the integral equation for the control volumes. Applying Eq. (14) for a *SCV* with three discrete *SS*s, shown in Fig. 1(b), and using an implicit time integration produces the following equation;

$$\begin{aligned}&\int\int_A \left(\frac{1}{\mu}[K].\nabla P\right).dA + \int\int_B \left(\frac{1}{\mu}[K].\nabla P\right).dB \\ &\quad + \int\int_C \left(\frac{1}{\mu}[K].\nabla P\right).dC + \delta \\ &\quad = V_{scv}\phi \frac{f_c - f_o}{\Delta t}\end{aligned} \tag{15}$$

in which *A*, *B* and *C* are the subsurfaces of a *SCV* (see Fig. 1b) and δ denotes the sum of flow rates on the other surfaces of the *SCV*. The pressure gradient term, ∇P, in the earlier equation is expressed in local coordinates as [20]:

$$\nabla P = \left[J^{-1}\right][S]\{P\} \tag{16}$$

for which linear shape functions will be used to calculate it.

The discretization of the governing equation leads to several integrals, which must be performed over the *SCV* surfaces. In this study, the continuous surface

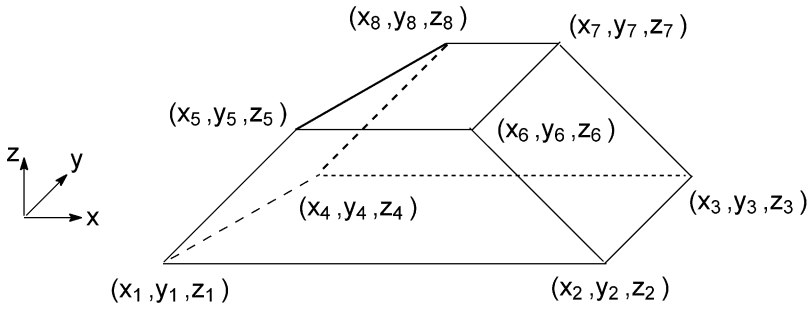

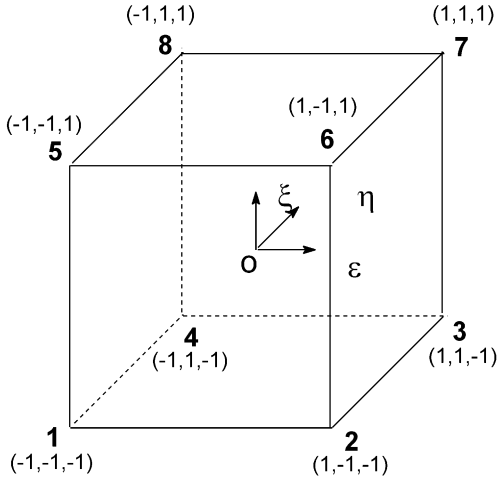

(a)

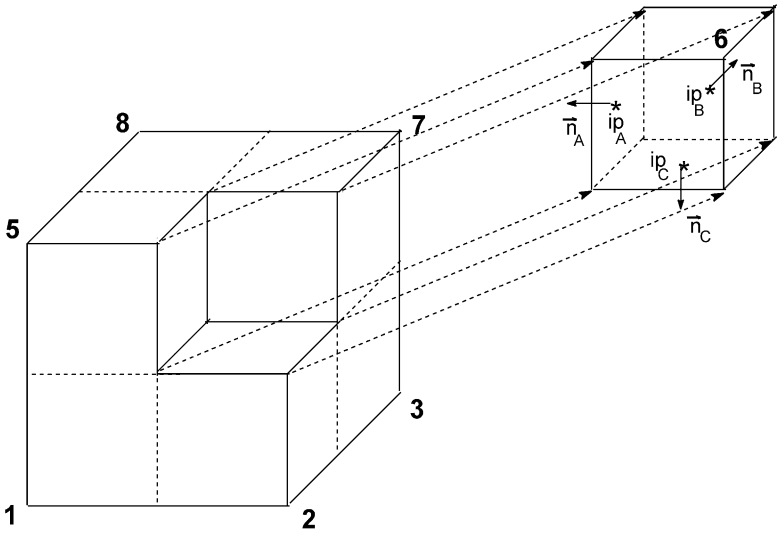

(b)

Fig. 1. (a) A typical eight-node hexahedral element in global and local coordinate systems and (b) a flux element divided into subcontrol volumes with one removed.

integration is approximated by evaluating them at a point called integration point (*ip*), that is located at the middle of any *SCV* subsurface, see Fig. 1(b). In this approximation, the integral argument is assumed to vary linearly and therefore the integrals are replaced by the flux terms evaluated at the *ip* times their subsurface area [28,29]. This approximation can help to further simplify the discretized equation. On the basis of this approximation and using Eq. (16), we would obtain the following relation for subsurface A:

$$\begin{aligned}&\int\int_A \left(\frac{1}{\mu}[K].\nabla P\right).dA \\ &\quad = \frac{1}{\mu_{ip_A}} < A > [K]_{ip_A}\left[J^{-1}\right]_{ip_A}[S]_{ip_A}\{P\}\end{aligned} \tag{17}$$

where $<A>$ denotes the vector of subsurface A in x, y, and $z$directions ($<A> = <A_x\ A_y\ A_z>$) and ip_A represents the *ip*value of the matrices. Applying this procedure for subsurfaces B and C, and summing all terms in an appropriate manner, the discretized equation for a *SCV* is expressed as follows:

$$\begin{aligned}&\left\{\frac{1}{\mu_{ip_A}} < A > [K]_{ip_A}\left[J^{-1}\right]_{ip_A}[S]_{ip_A}\right. \\ &\quad + \frac{1}{\mu_{ip_B}} < B > [K]_{ip_B}\left[J^{-1}\right]_{ip_B}[S]_{ip_B} \\ &\quad \left. + \frac{1}{\mu_{ip_C}} < C > [K]_{ip_C}\left[J^{-1}\right]_{ip_C}[S]_{ip_C}\right\}\{P\} + \delta \\ &\quad = V_{SCV}\phi\frac{f_c - f_o}{\Delta t}\end{aligned} \tag{18}$$

Since the assembling of global matrix is performed based on the elemental concept, the following closed form relation can be expressed for an arbitrary element in the solution domain:

$$\begin{aligned}&\sum_{i=1}^{8}\left\{\left(\frac{1}{\mu_{ip_A}} < A > [K]_{ip_A}\left[J^{-1}\right]_{ip_A}[S]_{ip_A}\right.\right. \\ &\quad + \frac{1}{\mu_{ip_B}} < B > [K]_{ip_B}\left[J^{-1}\right]_{ip_B}[S]_{ip_B} \\ &\quad \left.\left. + \frac{1}{\mu_{ip_C}} < C > [K]_{ip_C}\left[J^{-1}\right]_{ip_C}[S]_{ip_C}\right)\{P\}\right\}_i \\ &\quad + \sum_{i=1}^{8}\delta_i = \sum_{i=1}^{8}\phi V_{SCV,i}\frac{f_{c_i} - f_{o_i}}{\Delta t}\end{aligned} \tag{19}$$

where the $\sum_{i=1}^{8}\delta_i$ denotes the additional flux terms coming from each *SCV* in an element. Since this term is vanished for a *CV*, it will be ignored during the global matrix assembly. Eq. (19) is applied to all elements within the solution domain, and applying an appropriate assembly procedure results in a set of nonlinear algebraic equations for pressure. In matrix notation, it can be expressed as:

$$\boldsymbol{A}\ \boldsymbol{P} = \boldsymbol{F}_c - \boldsymbol{F}_o \tag{20}$$

in which components of $\boldsymbol{F}$ is related to fill fraction field $\boldsymbol{f}$ at a *CV* as:

$$F_i = \frac{\phi V_i f_i}{\Delta t} \tag{21}$$

Substituting Eq. (21) into Eq. (20) and rearranging the resulted equation, we get:

$$\boldsymbol{A}'\boldsymbol{P} = \boldsymbol{f}_c - \boldsymbol{f}_o \tag{22}$$

where components of $\boldsymbol{A}'$ are related to matrix $\boldsymbol{A}$ in Eq. (20) through the following expression:

$$A_i^{'} = \frac{\Delta t}{\phi V_i}A_i \tag{23}$$

in which A_i represents the components of ith row in matrix A and $A_i^{'}$ is its correspondence in Eq. (22). Eq. (22) is a working equation to find the pressure and fill fraction field on the basis of nodal partial saturation concept. A set of nonlinear equations obtained by Eq. (22) are solved by an appropriate solution procedure and having satisfied the following conditions:

$$\begin{aligned}&\text{For all nodes;}\quad P \geqslant 0 \\ &\text{For all nodes where } 0 \leqslant f < 1;\quad P = 0 \\ &\text{For all nodes;}\quad 0 \leqslant f \leqslant 1\end{aligned} \tag{24}$$

In order to obtain a working equation for quasi-steady state approach, one can start the earlier-mentioned procedure for Eq. (6). The resultant equation is as:

$$\boldsymbol{A}\ \boldsymbol{P} = \boldsymbol{0} \tag{25}$$

where components of $\boldsymbol{A}$ is the same as Eq. (20). Eq. (25) is the working equation to find the pressure and fill fraction filed on the basis of quasi-steady state concept.

3.2. Energy and chemical species equations

Integration of Eq. (8) over a *CV* with the aid of Divergence theorem gives:

$$\begin{aligned}&\frac{\partial}{\partial t}\int\int\int_V \rho C_p T dV \\ &\quad + \int\int_S \rho_r C_{p_r}\left(\vec{v}\ .\vec{n}\right)\boldsymbol{dS}\int\int_S \vec{n}\ .k\nabla T\ \boldsymbol{dS} \\ &\quad + \int\int\int_V \phi\Delta H\dot{G}dV\end{aligned} \tag{26}$$

Similar to the procedure described for the flow model and using the implicit method for a given time step, Eq. (26) is approximated for a *SCV* as:

$$\frac{\rho C_p V_{scv}}{\Delta t}\left(T^{n+1}-T^{n}\right)+\rho_r C_{p_r}\left\{<A>\vec{v}_{ip_A}\,T^{n+1}_{ip_A}+<B>\vec{v}_{ip_B}\,T^{n+1}_{ip_B}+<C>\vec{v}_{ip_C}\,T^{n+1}_{ip_c}\right\}+\delta_T=\left\{k_{ip_A}<A>\left[J^{-1}\right]_{ip_A}[S]_{ip_A}+k_{ip_B}<B>\left[J^{-1}\right]_{ip_B}[S]_{ip_B}+k_{ip_C}<C>\left[J^{-1}\right]_{ip_C}[S]_{ip_C}\right\}\{T^{n+1}\}+\phi V_{SCV}\Delta H\dot{G} \tag{27}$$

Like Eq. (16), temperature gradient term has been used as follows:

$$\nabla T=\left[J^{-1}\right][S]\{T\} \tag{28}$$

According to the approach used to make the global matrix of the flow model, the following closed form relation is obtained for each arbitrary element in the solution domain:

$$\sum_{i=1}^{8}\frac{\rho C_p V_{SCV,i}}{\Delta t}\left(T_i^{n+1}-T_i^{n}\right)+\sum_{i=1}^{8}\rho_r C_{p_r}\left\{<A>\vec{v}_{ip_A}\,T^{n+1}_{ip_A}+<B>\vec{v}_{ip_B}\,T^{n+1}_{ip_B}+<C>\vec{v}_{ip_C}\,T^{n+1}_{ip_c}\right\}_i+\sum_{i=1}^{8}\delta_{Ti}=\sum_{i=1}^{8}\left\{\left(k_{ip_A}<A>\left[J^{-1}\right]_{ip_A}[S]_{ip_A}+k_{ip_B}<B>\left[J^{-1}\right]_{ip_B}[S]_{ip_B}+k_{ip_C}<C>\left[J^{-1}\right]_{ip_C}[S]_{ip_C}\right)\{T^{n+1}\}\right\}_i+\sum_{i=1}^{8}\phi V_{SCV,i}\Delta H\dot{G}_i \tag{29}$$

Likewise, the discretized equation for chemical species equation can be expressed as:

$$\sum_{i=1}^{8}\frac{\phi V_{SCV,ii}}{\Delta t}\left(\alpha_i^{n+1}-\alpha_i^{n}\right)+\sum_{i=1}^{8}\left\{<A>\vec{v}_{ip_A}\,\alpha^{n+1}_{ip_A}+<B>\vec{v}_{ip_B}\,\alpha^{n+1}_{ip_B}+<C>\vec{v}_{ip_C}\,\alpha^{n+1}_{ip_c}\right\}_i+\sum_{i=1}^{8}\delta_{c_i}=\sum_{i=1}^{8}\phi V_{SCV,i}\dot{G}_i \tag{30}$$

Applying Eqs. (20) and (30) to all elements within the solution domain leads to the following set of equations for heat transfer and species balances, respectively:

$$\boldsymbol{A}^{\boldsymbol{T}}\boldsymbol{T}=\boldsymbol{B}^{\boldsymbol{T}} \tag{31}$$

$$\boldsymbol{A}^{\boldsymbol{\alpha}}\boldsymbol{\alpha}=\boldsymbol{B}^{\boldsymbol{\alpha}} \tag{32}$$

Eqs. (31) and (32) are the governing equations to solve the temperature and conversion in filled region. It is seen that these equations involve the integration point values of temperature and conversion in convection terms. Therefore, it needs to determine the integration point value in terms of nodal values. In order to do so, we use the modified linear profile version of skewed upstream differencing scheme [30]. The upstream of the streamline passing through the integration point intersects the element face (see Fig. 2). The integration point values in Eqs. (29) and (30) are then replaced by the value of this quantity at the intersection point named φ. The value of φ is related to the nodal values using a linear interpolation on the element face. To reduce the risk of producing negative coefficient in this method and increase the stability and accuracy, a modification is made in the interpolation coefficient obtained earlier. For this, any nodal dependence of φ on nodes that are on the downstream side of the integration point are replaced with an equal dependency of the nearest node within the element that is on the upstream side of the integration point. This significantly reduces the effect of negative coefficient on predicted value of temperature and conversion.

As illustrated earlier, we use an implicit time integration method in energy and chemical species equations. This guarantees the linear stability of the method unconditionally. However, if large time steps are used in flow equation based on nodal partial saturation formulation presented earlier, leading to large truncation

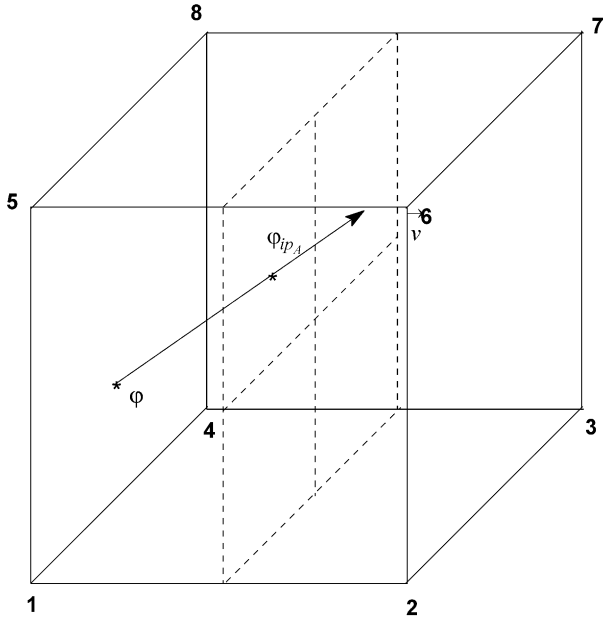

Fig. 2. Upstream value of an integration point obtained from intersection of streamline passing from an integration point, with an element face.

error and meaningless solutions of temperature and conversion. Furthermore, large time step suffers diffusion errors. In order to remove this difficulty, it is more appropriate to subdivide the time step used for the flow equation into smaller sub-times in energy and chemical species equations. The number of sub-time steps in each time step may be obtained by the following expression [2]:

$$N = Int\left(\frac{\psi_{\max}}{\gamma}\right) \tag{33}$$

in which the constant value γ should be between 0.7 and 1.1 for the best accuracy. The Courant number in an element is given by:

$$\psi^e = \frac{\left|\vec{v}\right|\Delta t}{\Delta l} \tag{34}$$

where Δl is the smallest side of an element. The time step,Δt, is calculated in quasi-steady state formulation but it is selected in the nodal partial saturation approach presented in this paper. The maximum value of Courant number calculated by Eq. (34) for all elements within the solution domain is used to obtain N in Eq. (31). Lin et al. [2] used this approach for their numerical solution based on quasi-steady state formulation. We have used this procedure in both quasi-steady state and nodal partial saturation formulations. In our experience, the sub-time method is more efficient for partial saturation formulation in which the selected time step is usually larger than the value obtained from quasi-steady state approach. In most simulations performed using quasi-steady state procedure, N was small.

4. Numerical schemes for non-isothermal mold filling

Two algorithms are presented to track the flow front in simulation of non-isothermal mold filling of the RTM process: one is based on quasi-steady state approach and the other one is based on the concept of nodal partial saturation at flow front. The resulting codes are named N-RTMS and N-RAPFIL, respectively. Both computer programs are written in FORTRAN 77.

4.1. Quasi-steady state approach

Eqs. (25), (31) and (32) are the working equations in this approach. The steps involved in the present numerical scheme are:

Step 1: At the beginning of the simulation, the pore volume of control volumes formed from element *SCVs* around each node is calculated. For the first time step, it is assumed that control volumes associated with the inlet nodes are fully filled with resin. It means that the fill fraction for these nodes are set to 1 and these nodes are considered as the solution domain.
Step 2: The nodal resin viscosity is calculated using a set of initial guessed values of temperature and conversion. The temperature and conversion distributions obtained from the previous time step are then used as the first guess at present time step. With these values, the stiffness matrix is assembled and the nodal pressures are calculated.
Step 3: Velocity field for filled region is obtained using the pressure distribution calculated in step 2 and the previous value of viscosity. Then, maximum Courant number and the number of sub-time steps are obtained using Eqs. (33) and (34).
Step 4: Temperature and conversion distributions are calculated for each sub-time step. Since energy equation and mass equation are interrelated through reaction rate, G, an iterative solution procedure is used to obtain the temperature and conversion at the end of sub-time step. However, it was observed that they converge after approximately <4 iterations.
Step 5: The value of nodal viscosity is updated based on the new temperature and conversion distributions.
Step 6: The new value of viscosity distribution obtained in step 5 is used to recalculate the pressure, temperature and conversion distributions using steps 2–5. This procedure is repeated until the relative error between new and old value of viscosity falls below a user-defined convergence criteria.

Step 7: When the convergence of viscosity is reached, new flow front and time step are calculated using the following equation:

$$V_i f_i^{t+\Delta t} = V_i f_i^t + \sum_{m=1}^{M} q_{mi}\Delta t \tag{35}$$

where q_{mi} is the flow rate between adjacent control volumes from m to i and M is the number of control volumes surrounding control volume i. After computing the time step, the position of the flow front is obtained by interpolating the fill fraction field to determine the contour of its corresponding value, namely $f=0.5$.
Step 8: Steps 2–7 are repeated for the new solution domain until the mold is completely filled up.

4.2. Nodal partial saturation approach

The steps accounted for in the present numerical scheme are illustrated below.

Step 1: Repeat step 1 of the previous scheme.
Step 2: Repeat step 2 of previous scheme to calculate the viscosity distribution.

Step 3: Matrix A' is calculated by the viscosity value guessed in step 2 and selecting a time step (Δt). At the beginning of iteration, f_c is initialized with f_o (fill fraction field at the end of previous time step). After imposing the boundary conditions, in Eq. (22), the resultant set of equations are solved to find the nodal pressure. Using the calculated nodal pressure, fill fraction field, f_c , is updated by unmodified Eq. (22). This procedure is repeated until the change in sum of the fill fractions between two iteration falls below a small user defined value. Then, the flow front is obtained by interpolating the fill fraction field for $f = 0.5$. Details of this step can be found elsewhere [20,21].

Step 4: Step 3 is only used to determine the fill fraction field for a selected time step. After this, the pressure field is calculated from the solution of the following equations:

$$A'P = 0 \tag{36}$$

To which the appropriate boundary conditions are applied. In this stage the pressure field for the filled region is determined at the end of each time step. Then velocity field and maximum Courant number are determined according to the procedure described in step 3 of previous scheme.

Step 5: Step 4 of previous scheme is carried out to calculate the temperature and conversion distributions.

Step 6: The nodal values of viscosity are updated based on the new temperature and conversion distributions.

Step 7: If viscosity has not converged, steps 2–6 are repeated to determine new flow front region, temperature and conversion distributions. This procedure is continued until the convergence criterion for viscosity is met.

Step 8: Steps 2–7 are repeated until the mold is completely filled up.

The flow charts of both numerical schemes are given in Figs. 3 and 4.

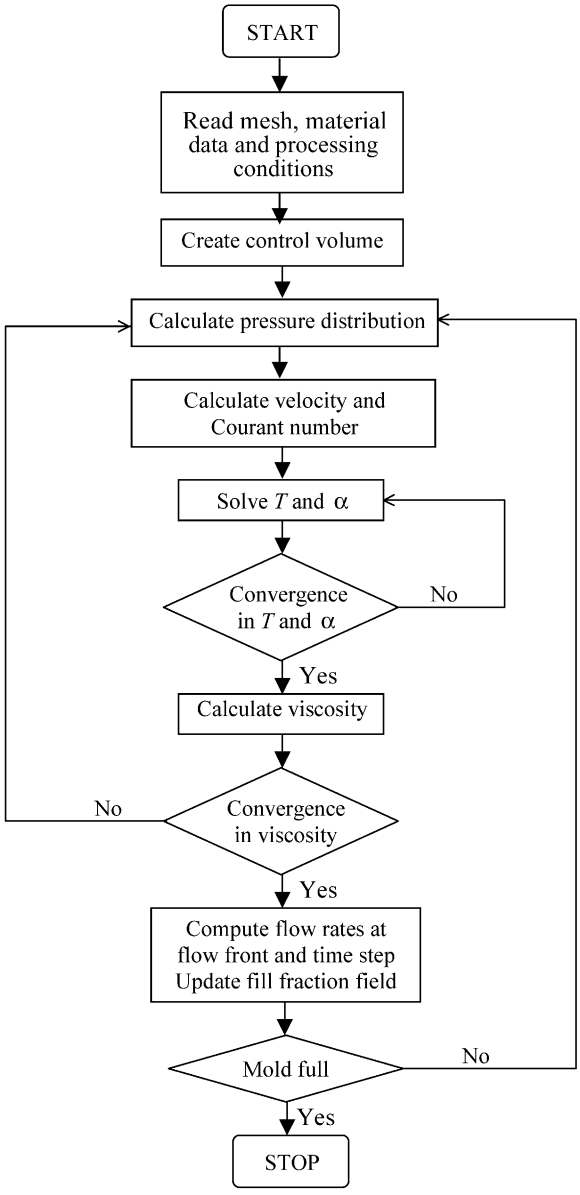

Fig. 3. Flow chart of the numerical scheme for N-RTMS.

5. Validation of the numerical simulations

The validity of the numerical codes presented earlier is checked with analytical solution of one-dimensional flow for both isothermal and non-isothermal flow conditions.

5.1. One-dimensional isothermal flow

The mold cavity used in this example is a rectangular cavity with the dimensions of 0.3, 0.1 and 0.002 m in length, width and thickness directions, respectively. The resin is injected at one surface of the rectangular mold and air is removed from the other surface resulting in one-dimensional flow. The analytical solution for flow front location under constant pressure injection is [31]:

$$x^2 = \frac{2KP_0}{\phi\mu}t \tag{37}$$

For the constant flow rate injection, the inlet pressure is determined from [31]:

$$P = \frac{\mu Q_0}{SK}x \tag{38}$$

The material properties and process parameters used in this example are listed in Table 1. In this example, number of elements along the width and thickness are two, and ten elements are used along the length. The

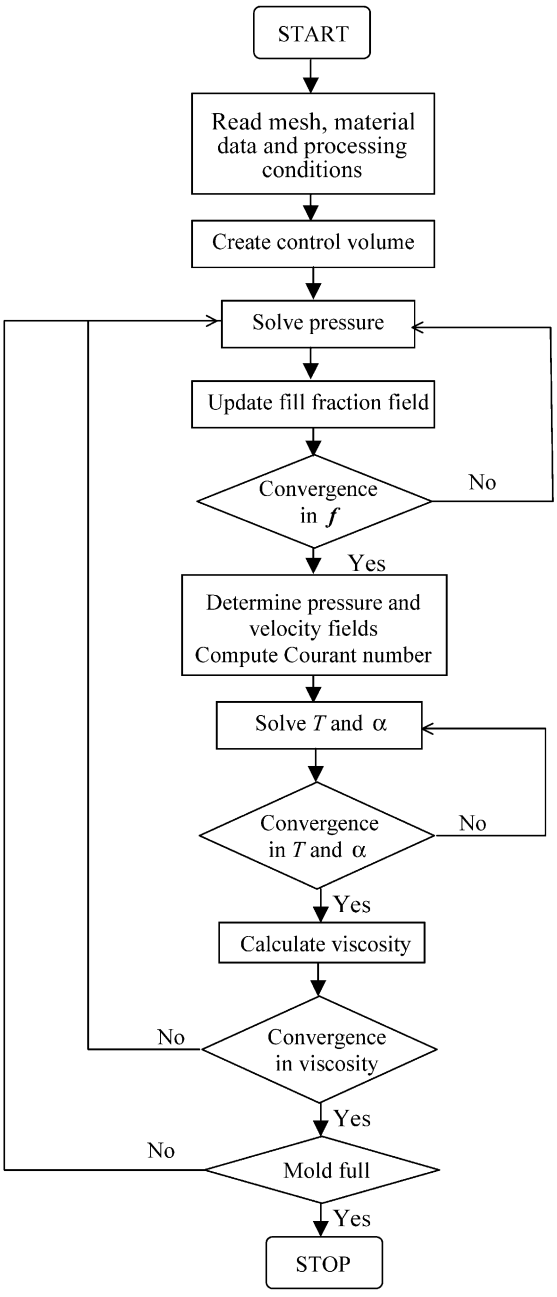

Fig. 4. Flow chart of the numerical scheme for N-RAPFIL.

comparison between the numerical and analytical results for both computer codes is shown in Fig. 5. The comparison is also performed for two different time steps for the N-RAPFIL. A small impregnation length is observed in the figure at the onset of filling process. This is due to the inlet control volumes that are assumed to be full at the beginning of the simulation. The results show accurate predictions made by both computer codes developed in this paper. The simulation results obtained by the N-RAPFIL in different time steps are the same as well.

5.2. One-dimensional non-isothermal flow

Analytical solution for the temperature profile in one-dimensional non-isothermal flow is given by:

$$\theta(x', y) = \sum_{n=0}^{\infty} \theta_0 \frac{2(-1)^n}{\lambda_n h} \exp\left(-\lambda_n^2 x'\right) \cos(\lambda_n y) \tag{39}$$

where $x' = \beta x/u$, $\theta = T - T_{\text{mold wall}}$ and $\lambda_n = (2n+1)\pi/2h$ in which h is half the mold gap. Bruschke and Advani [4] used this equation to validate their numerical simulation. The parameters of this test case are listed in Table 2. In this case, the resin is injected at one surface of the mold at temperature T_0 while the mold wall temperature is kept constant, $T_{\text{mold wall}}$. Like the previous example, the resulting flow will be also one-dimensional in this case. The dimensions of length, width and thickness of the mold cavity in this example are: 3, 1 and 2 m, respectively.

The mold cavity is discretized into 24 elements in length, four elements in width and six elements in thickness directions. Fig. 6 illustrates the analytical solution and numerical results for temperature profile at mid plane of the mold. In this example, two different time steps are used for the N-RAPFIL (see Fig. 6). As seen, the agreement between analytical solution and numerical results is very close. The maximum error in temperature is $<2\%$ for both computer codes. The results of the N-RAPFIL for two different time steps are also the same.

Table 1
Process parameters and material properties used in the one-dimensional isothermal flow simulation

Parameter	Value
Q_0 (m^3/s)	5×10^{-7}
P_0 (kPa)	150
μ (Pa s)	0.4
ϕ	0.5
K (m^2)	10^{-9}

Table 2
Process parameters and material properties used in the one-dimensional non-isothermal flow simulation [4]

Parameter	Value
h (m)	1
β (m/s)	1
U(m/s)	1
T_0 (°K)	273
$T_{\text{mold wall}}$ (°K)	373

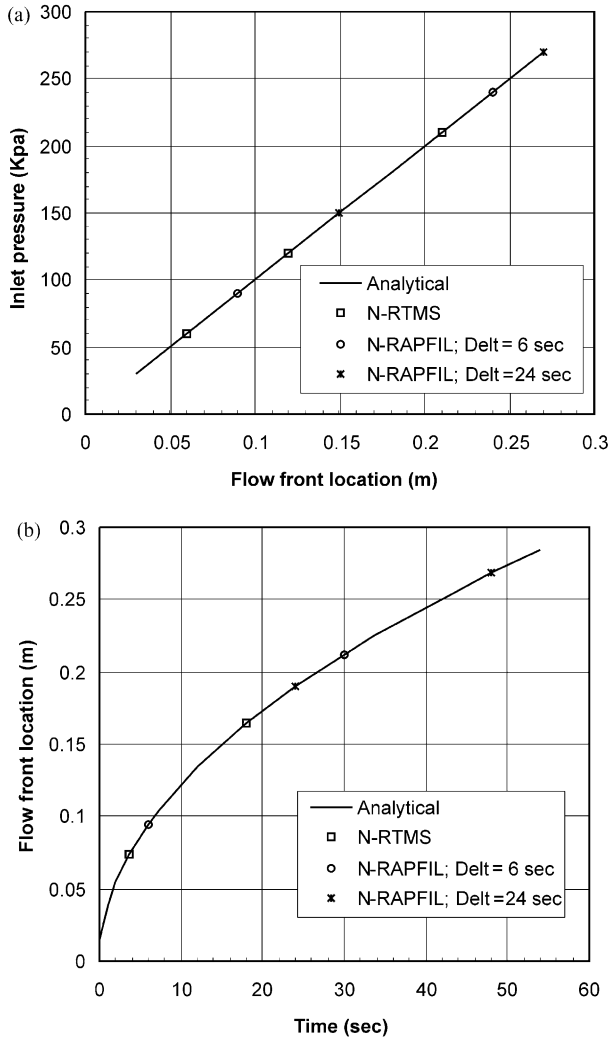

Fig. 5. Simulation results obtained from the N-RTMS and N-RAPFIL for one-dimensional isothermal flow; (a) inlet pressure under constant flow rate, (b) flow front location under constant pressure.

6. Numerical case studies

Three different cases are used to demonstrate applications of the computer codes developed in this study. The properties of resin and fiber used in these simulations are listed in Table 3. The kinetic and rheological parameters required for Eqs. (7) and (11) are taken from Ref. [2] and given in Table 4. In all cases resin is injected at 20 °C and the mold wall temperature is kept constant at 75 °C. The initial fiber mat temperature is set equal to the mold wall temperature.

The first case includes numerical simulation of the non-isothermal mold filling stage in a thin rectangular mold using N-RTMS and N-RAPFIL codes. Two different time steps are used for the N-RAPFIL; $\Delta t = 1$ s and $\Delta t = 3$ s. The dimensions of the mold cavity are: 0.2 m×0.08 m× 0.004 m. The resin is injected through a line gate located at center of the left side of the mold (see Fig. 7). The injection is performed under a constant flow rate with a value of 5.5×10^{-6} m^3/sec. The total number of nodes and elements for this test case are 735 and 480, respectively. Three different points inside the mold cavity are considered to compare their results computed from the two computer codes. The points are located at the mid plane of the mold with positions: A-1 (0.04, 0.04, 0.002 m) near the injection gate, B-1 (0.1, 0.04, 0.002 m) at the center and C-1 (0.13, 0.04, 0.002 m) near the end of mold. Fig. 8 shows the flow fronts predicted using the N-RTMS and N-RAPFIL. As expected in this case, the resin progresses as a plug flow due to small cavity thickness. As reported in Ref. [20], the predicted flow fronts by the N-RAPFIL with the two time steps are the same. As seen in the figure, the flow front locations resulted by both codes are reasonably close together.

Fig. 9 shows the predicted temperature histories of the three points during the mold filling stage. As shown in the figure, the temperature of a point decreases from the fiber mat temperature to an equilibrium temperature when the flow front passes that point. The point located far away from the gate has higher temperature than the point located near the inlet gate. This is due to the long residence time and the high temperature of the resin at the points located far away from the inlet gate. Fig. 9 also compares results of the two computer codes. As shown in the figure, the temperature histories predicted by both codes indicates the same trend and the results

Table 3
Properties of resin and fiber used in simulation

Parameter	Value
ρ_f	2560 kg/m^3
ρ_r	1100 kg/m^3
k_f	0.0335 W/m.°K
k_r	0.168 W/m.°K
C_{p_f}	670 J/kg.°K
C_{p_r}	1680 J/kg.°K
$K_{xx} = K_{yy} = K_{zz}$	2×10^{-9} m^2
ϕ	0.7

Table 4
Kinetic and rheological parameters used in simulation [2]

Parameter	Value
μ_0	2.78×10^{-4} Pa s
E_μ	18 000 J/mol
α_g	0.1
a	1.5
b	1
A_1	3.7833×10^{5} s^{-1}
A_2	6.7833×10^{5} s^{-1}
E_1	54 418 J/mol
E_2	50 232 J/mol
m_1	0.3
m_2	1.7
ΔH	1.54×10^{8} J/m^3

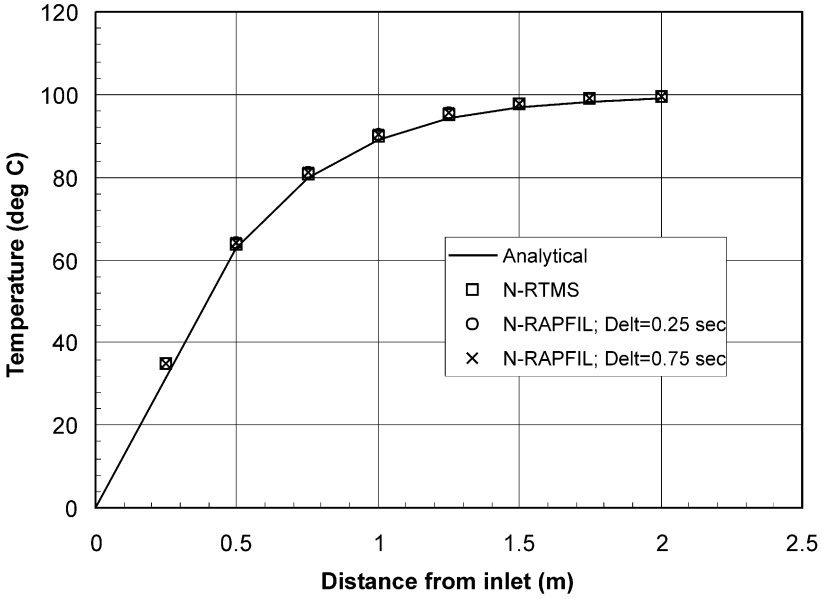

Fig. 6. Temperature profile along mid plane of the mold for non-isothermal test case.

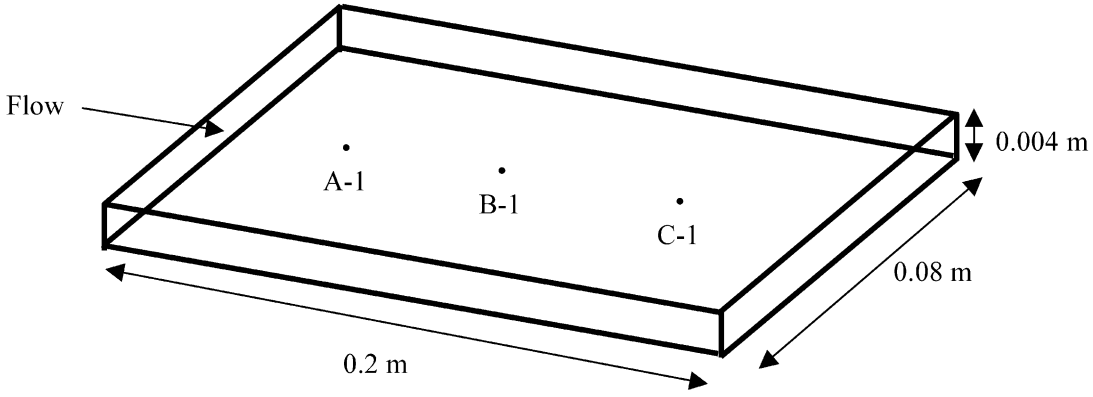

Fig. 7. Geometric details of rectangular mold.

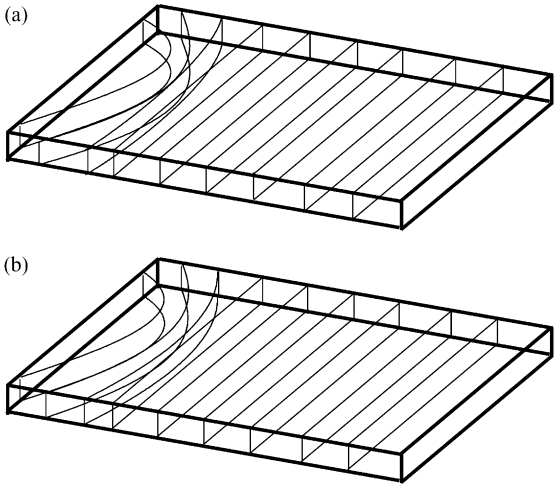

Fig. 8. Simulated flow front locations in a rectangular mold at equal time intervals of 1 s by (a) the N-RTMS and (b) the N-RAPFIL, $\Delta t = 1$and 3 s.

are very close. For the case of N-RAPFIL, the predicted temperature for large time step dose not change significantly, but the number of sub-time steps needed to simulate the temperature and conversion are increased.

Since the reaction rate strongly depends on the resin temperature, an accurate prediction of temperature distributions in the mold leads to a much better estimation of the resin cure. The predicted conversions near the end of mold filling process at the three points are illustrated in Table 5. As seen, the conversion at the last point, i.e. point C-1, is higher than the conversion at the first point, i.e. A-1, which is near the injection gate. This is due to the higher temperature of the farthest point from the gate. As illustrated in Table 5, the results of the two computer codes are very close.

The second geometry is a cubic mold with dimensions of 0.1 m×0.1 m× 0.1m which is shown in Fig. 10. Number of elements and nodes are 512 and 729, respectively. A point gate is located at a corner of the

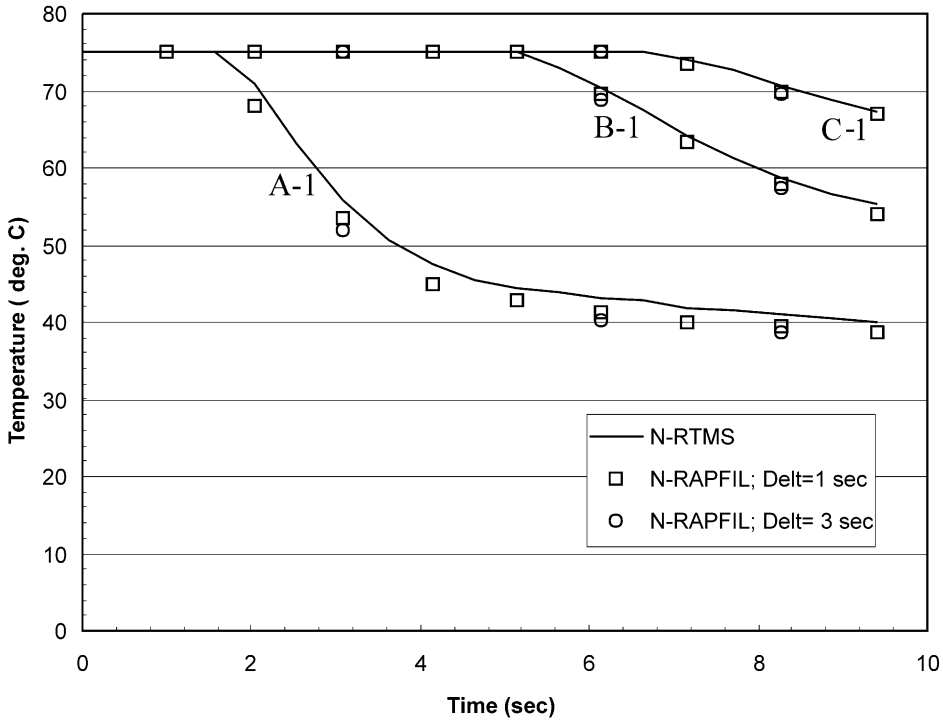

Fig. 9. Simulated temperatures of three different points, A-1, B-1 and C-1, in time in a rectangular mold by (a) the N-RTMS and (b) the N-RAPFIL, $\Delta t = 1$ and 3 s.

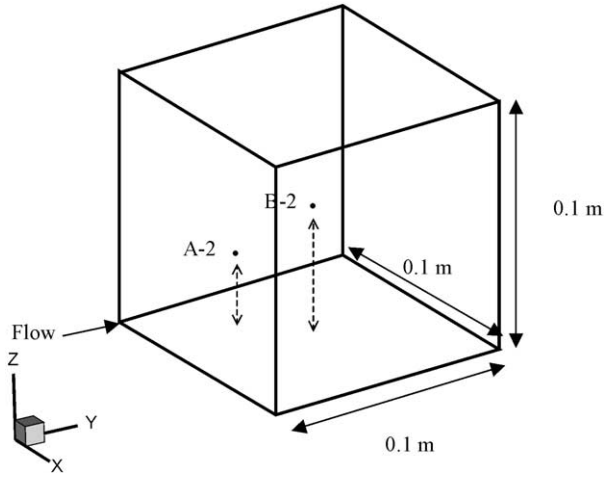

Fig. 10. Geometry of a cubic mold.

bottom surface of the mold. (see Fig. 10). The injection flow rate is 4.5×10^{-6} m^3/s in this test case. Fig. 11 shows the flow fronts simulated by N-RTMS and N-RAPFIL ($\Delta t = 1$ and 3 s). As shown in Fig. 11, the resin progresses from injection gate to the opposite corner of the mold at the top surface. Temperature histories at two points inside the mold are accounted for. The location of these points is shown in Fig. 10. Fig. 12 shows predicted temperature histories at the two points simulated by the N-RTMS and N-RAPFIL codes. Once again, the results obtained by the two codes are very close.

In order to illustrate the effectiveness of the computer codes further, a complicated geometry is considered as the third case. The geometric details of this mold cavity are shown in Fig. 13. The geometry is discretized into 1152 nodes and 736 elements. The resin is injected under constant flow rate of 6×10^{-6} m^3/s through a gate located at the top of the mold. The same analysis used for the cases one and two is also performed for this complicated geometry. Fig. 14 demonstrates the simulated flow front progression by both computer codes. The time step used for the N-RAPFIL in this test case is 0.5 s. Analytical mold filling time is simply calculated by dividing the pore volume of the cavity to the injection flow rate. Fig. 15 shows analytical and simulation

Table 5
Comparison of simulated conversion by the two computer codes near the end of mold filling at selected points in the rectangular mold

	Conversion (N-RTMS)	Conversion (N-RAPFIL, $\Delta t = 1$ s)	Conversion (N-RAPFIL, $\Delta t = 3$ s)
Point A-1	2.36×10^{-3}	2.2×10^{-3}	2.11×10^{-3}
Point B-1	1.17×10^{-2}	1.07×10^{-2}	1.05×10^{-2}
Point C-1	2.1×10^{-2}	1.99×10^{-2}	1.93×10^{-2}

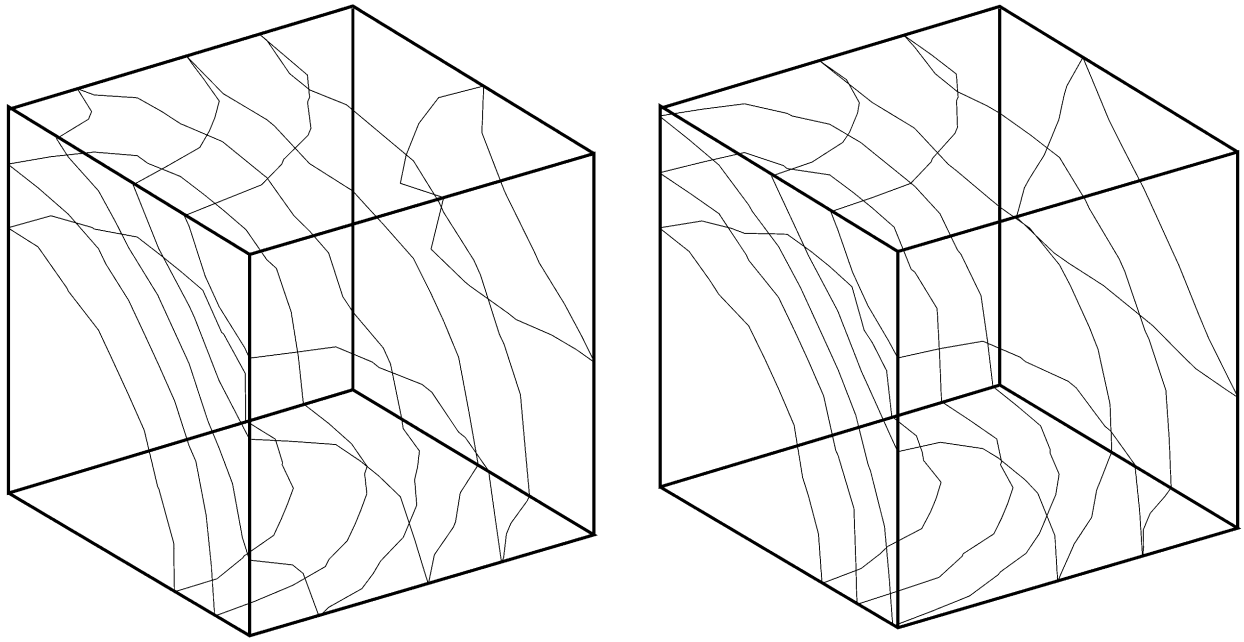

Fig. 11. Simulated flow front locations in a cubic mold at equal time intervals of 2 s by (a) the N-RTMS and (b) the N-RAPFIL, $\Delta t = 1$ and 3 s.

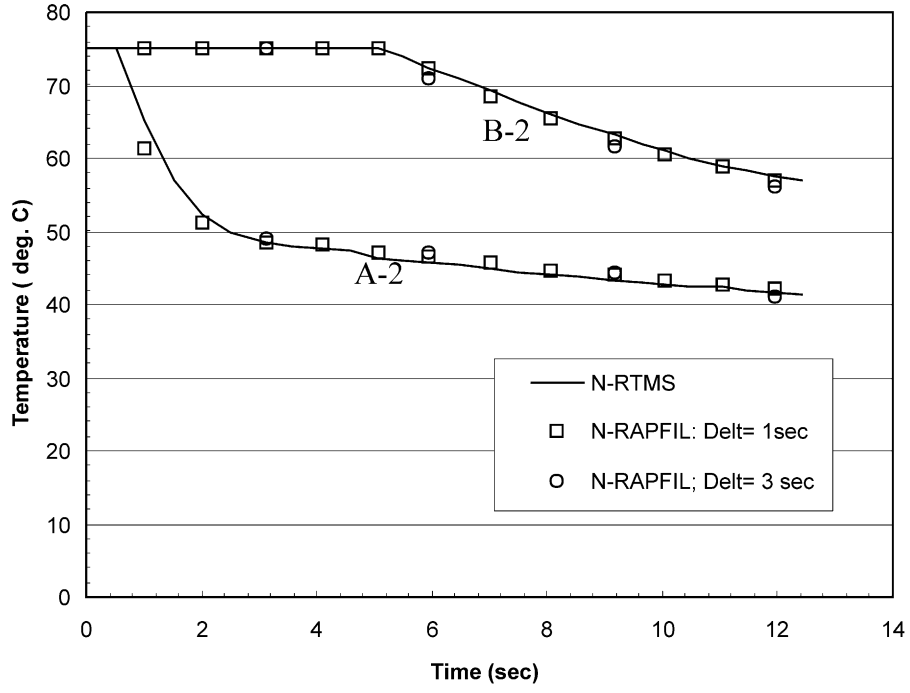

Fig. 12. Simulated temperatures of two different points, A-2 and B-2, in time in a cubic mold by (a) the N-RTMS and (b) the N-RAPFIL, $\Delta t = 1$ and 3 s.

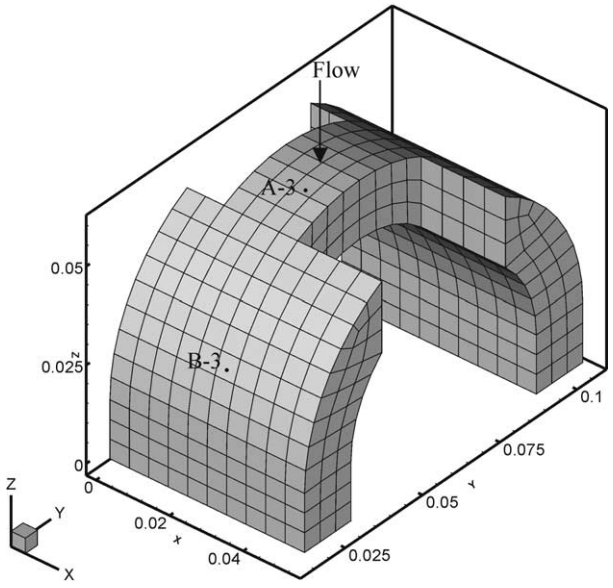

Fig. 13. Geometric details of complex shaped mold.

results of cavity fill fraction in time during the mold filling. The estimated error in filling time throughout the filling process is less than 0.1% for the N-RAPFIL and 1.5% for the N-RTMS. This indicates the higher accuracy of N-RAPFIL in calculation of filling time. The CPU time required for N-RAPFIL is about 40% less than the N-RTMS. This denotes the CPU effectiveness of the N-RAPFIL. Fig. 16 shows the temperature histories predicted by both computer codes at two selected points within the mold cavity. The predicted conversions at the end of mold filling are shown in Table 6 for the two points. The positions of these points are: A-3 (2×10^{-2} m, 5.46×10^{-2} m, 4.96×10^{-2} m) and B-3 (2.8×10^{-2} m, 2.685×10^{-2} m, 2.51×10^{-2} m), as shown in Fig. 13.

Table 6
Comparison of simulated conversion by the two computer codes near the end of mold filling at selected points in the complex shaped mold

	Conversion (N-RTMS)	Conversion (N-RAPFIL)
Point A-3	2.37×10^{-4}	2.654×10^{-4}
Point B-3	1.169×10^{-2}	1.14×10^{-2}

7. Conclusions

A computer code has been developed to simulate the three-dimensional non-isothermal mold filling in RTM based on the concept of nodal partial saturation at the flow front. The resulting computer code allows one to analyze the resin flow, temperature and conversion distributions in a three-dimensional space. This information is helpful to design of tooling and processing conditions before the mold is built. The simulation results obtained by the code has been compared with the conventional method based on the quasi-steady state formulation, which is implemented in this study as well. An excellent agreement is observed by comparing the results of both codes with analytical solutions. The examples presented in this paper illustrate the flexibility and effectiveness of the developed computer codes for

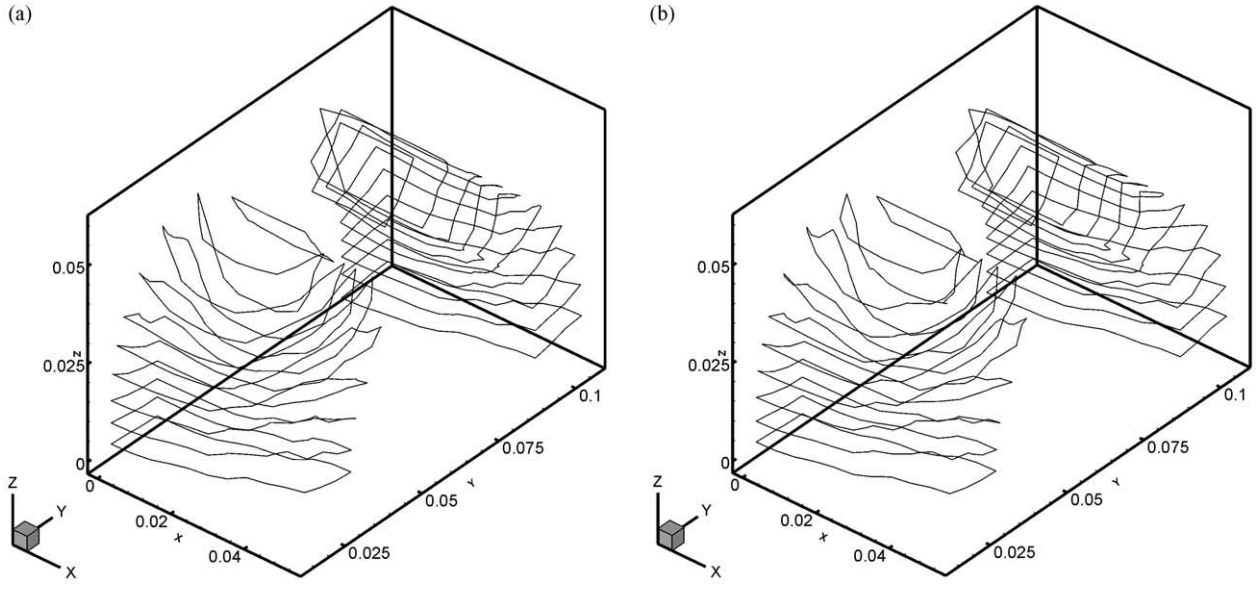

Fig. 14. Simulated flow front locations in a complex shaped mold at equal time intervals of 1 s by (a) the N-RTMS and (b) the N-RAPFIL, $\Delta t = 0.5$ s.

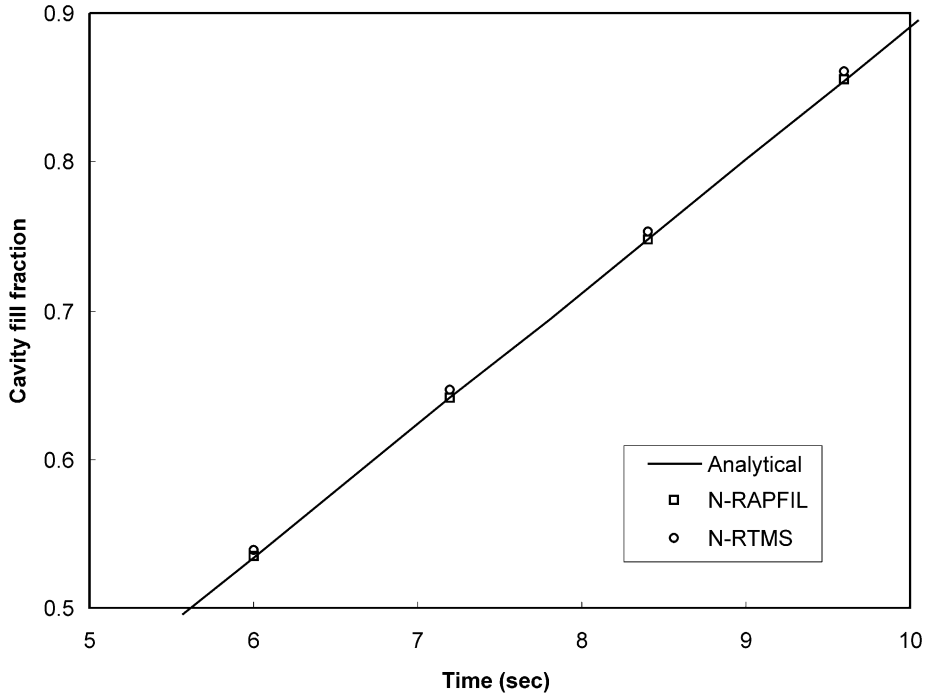

Fig. 15. Cavity fill fraction as function of time during mold filling for complex shaped mold.

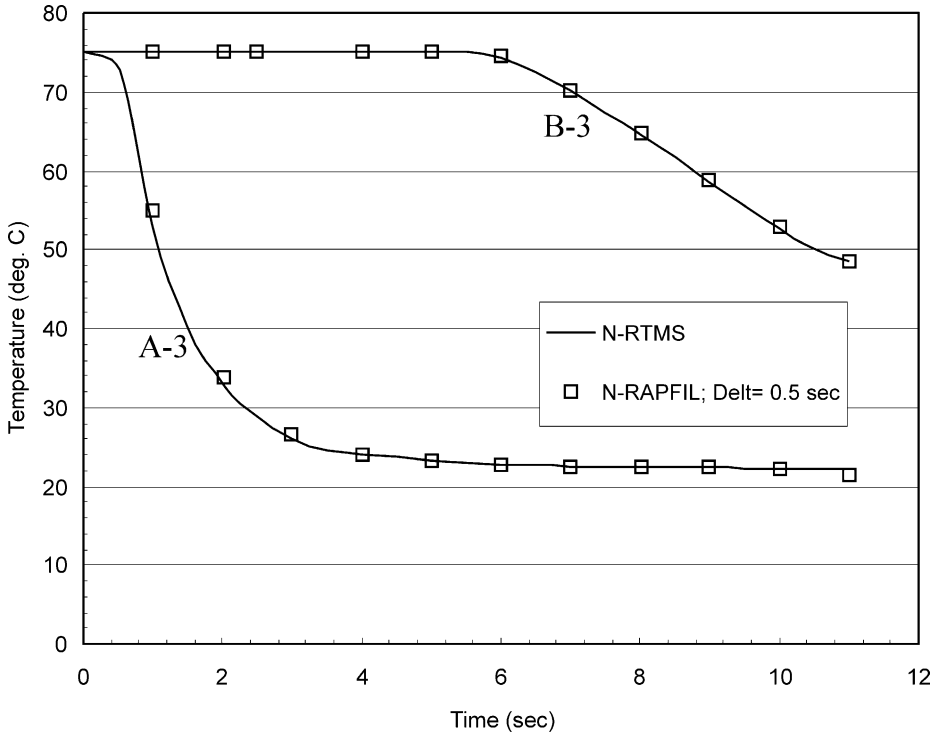

Fig. 16. Simulated temperatures of two different points, A-3 and B-3, in time in a complex shaped mold by (a) the N-RTMS and (b) the N-RAPFIL, $\Delta t = 0.5$ s.

simulation of complicated mold cavity. The results show that the developed computer code based on nodal partial saturation is stable and gives a reasonable result for simulation of the non-isothermal mold filling stage. It has been also shown that this scheme is more efficient than the conventional method from the viewpoint of the CPU time and gives rise more accurate prediction of filling process.

References

[1] Chan AW, Hwang ST. Modeling nonisothermal impregnation of fibrous media with reactive polymer resin. Polymer Engineering and Science 1992;32:310–8.

[2] Lin R, Lee LJ, Liou M. Non-isothermal mold filling and curing simulation in thin cavities with preplaced fiber mats. International Polymer Processing 1991;6:356–69.

[3] Hourng LW, Chang CY. Numerical simulation of resin injection molding in molds with preplaced fiber mats. Journal of Reinforced Plastics and Composites 1993;12:1081–95.

[4] Bruschke MV, Advani SG. A numerical approach to model non-isothermal viscous flow through fibrous media with free surfaces. International Journal For Numerical Methods in Fluids 1994;19: 575–603.

[5] Chan AW, Morgan RJ. Computer modeling of liquid composites molding for 3-dimensional complex shaped structures. In: Proceeding of the 10th Annual ASM/ESD Advanced Composites Conference 1994, Dearborn, Michigan 7–10 November 1994. p. 341–5.

[6] Gao DM, Trochu F, Gauvin R. Heat transfer analysis of non-isothermal resin transfer molding by finite element method. Materials and Manufacturing Processes 1995;10(1):57–64.

[7] Kang MK, Lee WI, Yoo JY, Cho SM. Simulation of mold filling process during resin transfer molding. Journal of Materials Processing and Manufacturing Science 1995;3:297–313.

[8] Mal O, Couniot A, Dupret F. Nonisothermal simulation of the resin transfer molding process. Composites Part A 1998;29:189–98.

[9] Lam YC, Joshi SC, Liu XL. Numerical simulation of the mold-filling process in resin-transfer molding. Composite Science and Technology 2000;60:845–55.

[10] Shojaei A, Ghaffarian SR, Karimian SMH. Modeling and simulation approaches in the resin transfer molding process—a review. Polymer Composites 2003;24(4).

[11] Young WB. Three-dimensional nonisothermal mold filling simulation in resin transfer molding. Polymer Composites 1994;15: 118–27.

[12] Lim ST, Lee WI. An analysis of the three-dimensional resin-transfer mold filling process. Composites Science and Technology 2000;60:961–75.

[13] Coulter JP, Guceri S. Resin impregnation during the manufacturing of composite materials subject to prescribed injection rate. Journal of Reinforced Plastics and Composites 1988;7:200–19.

[14] Gauvin R, Trochu F. Comparison between numerical and experimental results for mold filling in resin transfer molding. Plastics, Rubber and Composites processing and Applications 1993;19:151–7.

[15] Um MK, Lee WI. A study on the mold filling process in resin transfer molding. Polymer Engineering and Science 1991;31:765–71.

[16] Yoo YE, Lee WI. Numerical simulation of the resin transfer mold filling process using the boundary element method. Polymer Composites 1996;17:368–74.

[17] Joshi SC, Lam YC, Liu XL. Mass conservation in numerical simulation of resin flow. Composites- Part A: Applied Science and Manufacturing 2000;31:1061–8.

[18] Voller VR, Peng S. An algorithm for analysis of polymer filling of molds. Polymer Engineering and Science 1995;35:1758–65.

[19] Lin M, Hahn HT, Huh H. A finite element simulation of resin transfer molding based on partial nodal saturation and implicit time integration. Composites Part A 1998;29:541–50.

[20] Shojaei A, Ghaffarian SR, Karimian SMH. Numerical simulation of three-dimensional mold filling process in resin transfer molding using quasi-steady state and partial saturation formulations. Composites Science and Technology 2002;62:861–79.

[21] Shojaei A, Ghaffarian SR, Karimian SMH. Numerical simulation of three-dimensional mold filling in resin transfer molding. Journal of Reinforced Plastics and Composites [in press].

[22] Castro JM, Macosko CW. Studies of mold filling and curing in the reaction injection molding process. AICHE 1982;28:250–60.

[23] Advani SG, Bruschke MV. Resin transfer moulding flow phenomena in polymeric composites. Chapter 12. In: Advani SG, editor. Flow and rheology in polymer composites manufacturing. Amsterdam: Elsevier Science BV; 1994.

[24] Dessenberger RB, Tucker IIICL. Thermal dispersion in resin transfer molding. Polymer Composites 1995;16:495–506.

[25] Kamal MR, Sourour S. Kinetics and thermal characterization of thermoset resin. Polymer Engineering and Science 1973;13:59–64.

[26] Chan AW, Hwang ST. Mold-filling simulations for the injection molding of continuous fiber-reinforced polymer. Polymer Engineering and Science 1988;28:333–9.

[27] Antonucci V, Giordano M, Nicolais L, Di Vita G. A simulation of the non-isothermal resin transfer molding process. Polymer Engineering and Science 2000;40:2471–81.

[28] Schneider GE, Zedan M. Control-volume based finite-element formulation of the heat conduction equation. Spacecraft Thermal Control, Design, and Operation, Progress in Astronautics and Aeronautics 1983;86:305–27.

[29] Schneider GE, Raw MJ. Control volume finite-element method for heat transfer and fluid flow using collocated variables—1. Computational procedure Numerical Heat Transfer 1987;11:363–90.

[30] TASCflow version 2.3, Theory documentation. Advanced Scientific Computing Ltd 1994.

[31] Cai Z. Simplified mold filling simulation in resin transfer molding. Journal of Composite Materials 1992;26:2606–29.